ACS OMEGA

Open Access

http://pubs.acs.org/journal/acsodf

Article

Alkaline Earth Bismuth Fluorides as Fluoride-Ion Battery Electrolytes

Spencer Doyle, Edvin Tewolde Berhane, Peichao Zou, Ari B. Turkiewicz, Yang Zhang, Charles M. Brooks, Ismail El Baggari, Huolin L. Xin, and Julia A. Mundy*

Cite This: *ACS Omega* 2024, 9, 39082−39087

Read Online

ACCESS | Metrics & More | Article Recommendations | Supporting Information

ABSTRACT: Fluoride-ion batteries have several potential advantages over lithium-ion batteries. Materials development is still needed, however, to realize electrolytes with sufficiently high anion conductivity and compatibility with anode and cathode layers. Fluoride compounds are difficult to synthesize directly as single crystals but can be realized from oxide film precursors via topotactic chemistry techniques. Here, we create crystalline alkaline earth bismuth fluoride films $BaBiF_5$ and $SrBiF_5$ through oxide molecular beam epitaxy and topotactic fluorination. We characterize their ionic conductivities and demonstrate their potential as electrolytes. Finally, we realize epitaxial synthesis of $BaBiF_5$ on BaF_2 substrates, providing a route to thin film fluoride-ion battery devices.

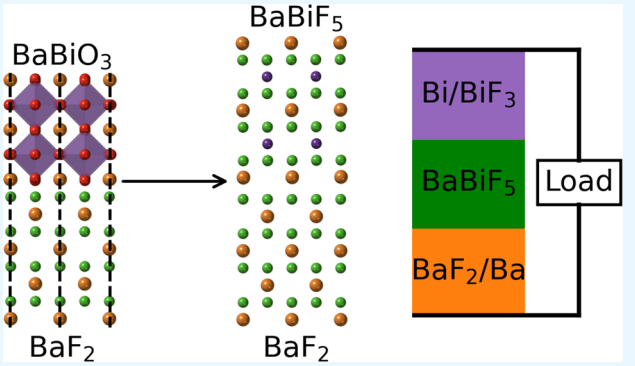

INTRODUCTION

Major economies around the world are in the process of transitioning away from fossil fuels and toward sustainable energy generation technologies. A substantial barrier in this transition is the inherent intermittency of renewable generation mechanisms. Grid-scale chemical batteries are expected to help address this issue by providing temporary energy storage, thus smoothing the variable output of renewables. Although elegant in theory, the expected scale of the required energy storage to stabilize target renewable portfolios is massive.[1] Lithium-ion batteries are by far the most prominent battery chemistry today. However, global lithium supply is likely to fall short of demand in this century.[2] Additionally, lithium is highly concentrated geographically, which introduces complex geopolitical factors.[3]

Fluorine is a particularly desirable charge carrier for batteries: global fluorine production is about one hundred times greater than that of lithium; CaF_2, the dominant naturally occurring fluoride mineral, makes for an excellent conversion-based anode material; and fluoride-ion batteries are predicted to have higher energy densities than lithium-ion batteries.[4] A battery based on fluoride ions was first reported in 2011.[5] A major limitation today for fluoride-ion batteries is the development of electrolytes with sufficient room temperature conductivity and that integrate well with anode and cathode materials. Many electrolyte candidates require temperatures around 150 °C or higher, although sufficient room temperature conductivity for battery cell operation was recently demonstrated.[6] In general, there remains a lack of viable electrolyte candidates.[7]

One way of identifying potential electrolyte materials is by taking inspiration from existing anode and cathode structures. Alkaline earth fluoride compounds CaF_2 and SrF_2 are commonly used anodes in fluoride-ion batteries. Additionally, BiF_3 is both relatively cheap and demonstrates lower volume change between charged and discharged states compared to other cathode materials.[4] A natural electrolyte in a battery using these anode and cathode choices would be an alkaline earth bismuth fluoride. Previous work on Ba−Bi−F compounds demonstrated a solid solution $BaBiF_5$ phase with a fluorite-type crystal structure.[8,9] More recently, Chikamatsu et al. realized single-crystal thin films of $BaBiF_5$ on $SrTiO_3$ substrates by performing a two-step synthesis process: topotactic fluorination of $BaBiO_3$ films synthesized by pulsed laser deposition.[10] However, ionic conductivity measurements have not been reported on such films. Here, we construct thin films of alkaline earth bismuth flourides and characterize their ionic conductivity. We start by synthesizing thin film perovskite oxides $BaBiO_3$ and $SrBiO_3$ by reactive oxide molecular beam epitaxy (MBE) on $SrTiO_3$ and BaF_2 substrates. We then perform topotactic fluorination on our oxide films, forming fluorite-type phases $BaBiF_5$ and $SrBiF_5$.[10−13] Finally, we characterize the ionic conductivity in these compounds to quantify their ability to function as fluoride-ion battery electrolytes, establishing the basis for

Received: June 24, 2024
Revised: August 1, 2024
Accepted: August 19, 2024
Published: September 2, 2024

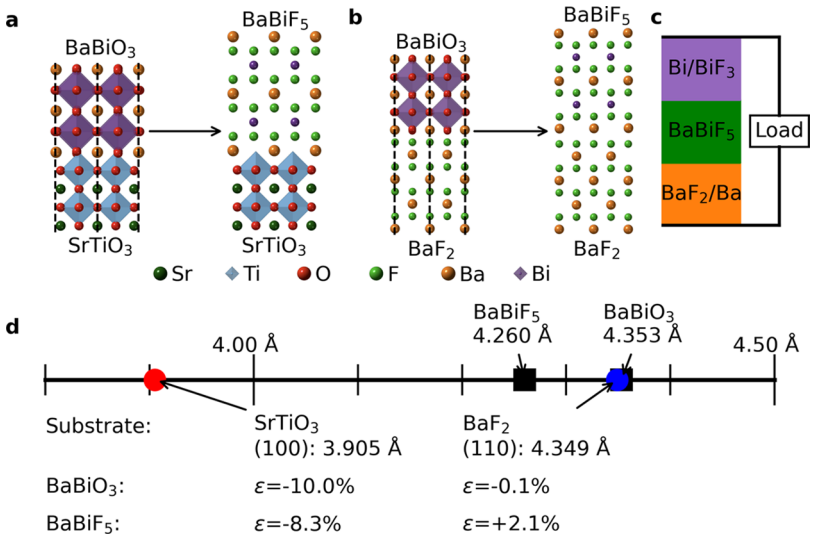

Figure 1. Creation of $BaBiF_5$ films on $SrTiO_3$ and BaF_2 substrates. (a) Demonstration of structural change from $BaBiO_3$ to $BaBiF_5$ on a $SrTiO_3$ substrate. The black dashed lines emphasize the in-plane mismatch between film and substrate. (b) The same structural conversion but on a BaF_2 substrate. Note the matched in-plane spacing between film and substrate due to strain. (c) Proposed three-element fluoride-ion battery stack consisting of BaF_2/Ba as a conversion-type anode, Bi/BiF_3 as a conversion-type cathode, and $BaBiF_5$ as an electrolyte. (d) Visualization of the difference between $SrTiO_3$ and BaF_2 substrates in terms of in-plane lattice parameters. $SrTiO_3$ has a much smaller in-plane spacing than both $BaBiO_3$ and $BaBiF_5$, whereas BaF_2 lies in between the two, allowing for strained films.

simple fluoride-ion battery stacks consisting of just three elements.

EXPERIMENTAL SECTION

Thin Film Synthesis. (100)-oriented $SrTiO_3$ substrates were purchased from OST Photonics. They were cleaned with acetone, isopropyl alcohol, and deionized water, and subjected to an anneal in air at 1000 °C for 4 hours. The resulting substrates demonstrated step terraces with widths on the order of 1 μm. (100)-oriented Nb-doped $SrTiO_3$ substrates were purchased from OST Photonics and subjected to the same treatment process described above for undoped $SrTiO_3$ substrates. (100)-oriented BaF_2 substrates were purchased from MSE Supplies. We did not treat these substrates due to the moisture sensitivity of BaF_2. The BaF_2 substrates demonstrated surface roughness of about 1.6 Å as measured by atomic force microscopy. Prior to the film deposition, barium, strontium, and bismuth fluxes were calibrated to be near 1×10^{13} atoms per square centimeter per second using a quartz crystal microbalance, and, in the case of barium, further optimized by tracking reflection high-energy electron diffraction oscillations for BaO.[14] A Riber Compact 21 molecular beam epitaxy chamber with a supplied 80% O_3/20% O_2 oxidant pressure around 2×10^{-6} Torr was used for film deposition. We synthesized $BaBiO_3$ and $SrBiO_3$ films using a codeposition process in which we provided roughly 50% excess bismuth for our highest quality samples (see Figure S1).

Topotactic Fluorination. Zinc fluoride powder of 99% purity from Sigma-Aldrich and poly(vinylidene fluoride) beads from Sigma-Aldrich were used as fluorination reagents. For the fluorination process, an oxide sample and approximately 0.1 g of reagent were placed in a tube about 1 cm apart from each other. Argon gas flowed through the tube at a rate of approximately 50 mL/min. The sample and reagent were then heated to 200 °C using a Thermo Scientific tube furnace and held at that temperature for 20 h. Longer fluorination processes resulted in no additional changes to the sample's X-ray diffraction (XRD) measurements.

Electrochemical Impedance Spectroscopy. Electrochemical impedance spectroscopy (EIS) data were collected using an electrochemical working station (Biologic) at the frequency range of 3 MHz to 0.1 Hz with an amplitude of 10 mV at varied temperatures ranging from about 20 °C (room temperature) to 90 °C. Ionic conductivities were measured along the crystallographic c-axis by sandwiching target fluoride films on conducting Nb:$SrTiO_3$ substrates between two stainless steel spacers, and then calculated according to $\sigma = L/R_bS$, where R_b is the resistance according to the EIS measurement, L is the thickness of the measured sample, and S is the effective contacting area between stainless steel spacers and samples. We note the lack of a linear low-frequency regime in our Nyquist plots, typically attributed to mass transfer phenomena. In this case, this may be due to a transmissive boundary at the film/substrate interface, or a constant phase element in the circuit, for example due to electrodes of differing surface roughness.[15,16]

RESULTS AND DISCUSSION

We represent the fluorination process visually in Figure 1. The structural change from perovskite $BaBiO_3$ to fluorite-type $BaBiF_5$ is shown on both $SrTiO_3$ (Figure 1a) and BaF_2 (Figure 1b) substrates. The out of plane lattice parameter increases from 4.33 to 6.04 Å, while the in-plane spacing decreases slightly from 4.35 to 4.26 Å.[10] Whereas $BaBiO_3$ films are known to relax on (100)-oriented $SrTiO_3$ due to the large lattice mismatch,[17] we find that the in-plane (110) direction of (100)-oriented BaF_2 substrates provides a close enough in-plane spacing to enable strained synthesis of $BaBiO_3$ (see Figure S2 for a schematic of the in-plane relationship). The relevant in-plane lattice parameters for $BaBiO_3$, $BaBiF_5$, $SrTiO_3$, and BaF_2 are shown in Figure 1d, along with the strain relationships between each substrate and the bismuth compounds. (100)-oriented BaF_2 is thus an optimal substrate

https://doi.org/10.1021/acsomega.4c05872
ACS Omega 2024, 9, 39082−39087

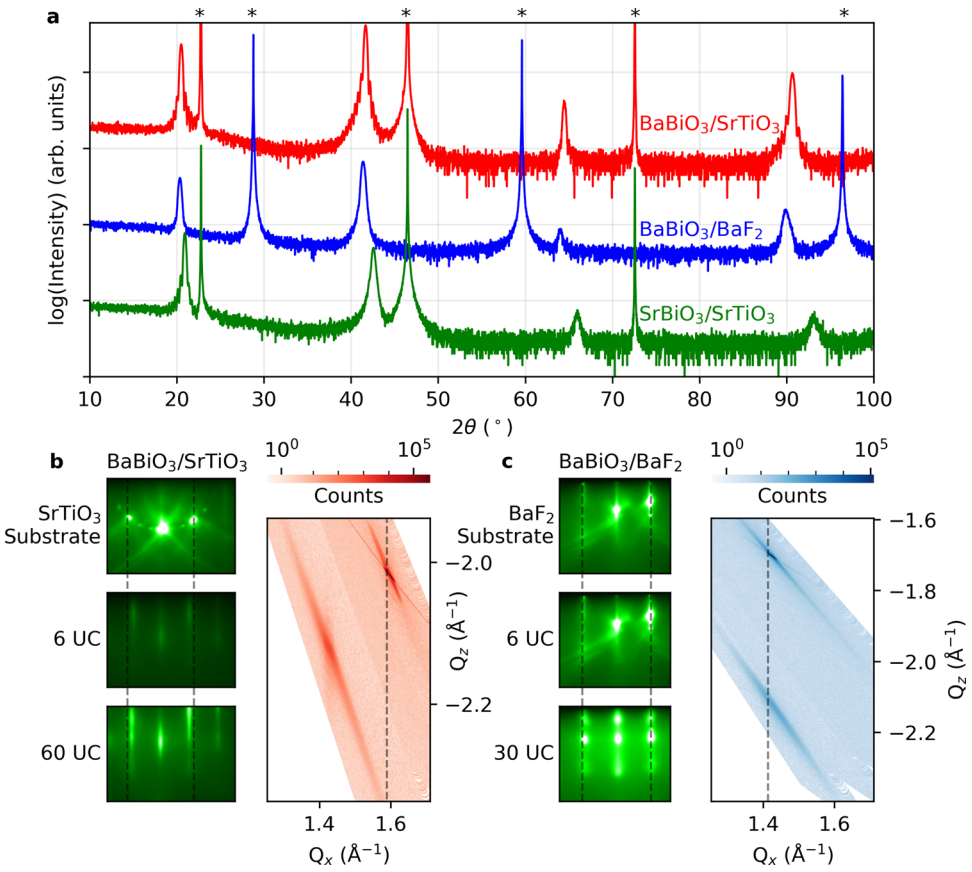

Figure 2. Synthesis of $BaBiO_3$ and $SrBiO_3$ thin films via molecular beam epitaxy. (a) X-ray diffraction measurements of three films: $BaBiO_3$ on a $SrTiO_3$ substrate (in red), $BaBiO_3$ on a BaF_2 substrate (in blue), and $SrBiO_3$ on a $SrTiO_3$ substrate (in green). Peaks denoted by asterisks at the top of the figure correspond to substrate diffraction. (b) On the left, RHEED images taken of a $BaBiO_3$ film on $SrTiO_3$ at various unit cells (UC) of deposition. On the right, an X-ray diffraction reciprocal space map of the film (206) peak (bottom left) near the substrate (103) peak (top right). The black dashed line corresponds to the $SrTiO_3$ substrate in-plane spacing. (c) On the left, RHEED images taken of a $BaBiO_3$ film on BaF_2. On the right, an X-ray diffraction reciprocal space map of the film (206) peak (bottom left) near the substrate (115) peak (top left). The black dashed line corresponds to the BaF_2 substrate in-plane spacing.

for this conversation, providing 0.1% compressive strain for $BaBiO_3$ and 2.1% tensile strain for $BaBiF_5$. Another advantage of BaF_2 is its potential to serve as a fluoride-ion battery anode. Alkaline earth fluoride compounds CaF_2 and SrF_2 perform well as anode materials in fluoride-ion batteries.[4,18] BaF_2 has the same cubic crystal structure as CaF_2 and SrF_2, so it is also a natural anode candidate. This provides the template for a simple fluoride-ion battery stack shown in Figure 1c: BaF_2 or SrF_2 as an anode, bismuth as a cathode, and $BaBiF_5$ or $SrBiF_5$ as an electrolyte.

We begin by synthesizing high-quality films of $BaBiO_3$ and $SrBiO_3$ by ozone-assisted molecular beam epitaxy. Our results are summarized in Figure 2. Previous studies demonstrated successful synthesis of these compounds on $SrTiO_3$ substrates, despite large 10 and 8% lattice mismatches with $BaBiO_3$ and $SrBiO_3$, respectively.[17,19,20] θ–2θ X-ray diffraction scans shown in Figure 2a demonstrate our high-quality films of $BaBiO_3$ and $SrBiO_3$ on $SrTiO_3$. We provide evidence of the lattice mismatch with both in situ electron diffraction and ex situ X-ray reciprocal space maps in Figure 2b. Tracking reflection high-energy electron diffraction (RHEED) during the deposition of $BaBiO_3$, we observed a blurring of the substrate diffraction spots (top image) in the first several unit cells. Starting at approximately unit cell five, film streaks begin to appear with a different diffraction spacing; the middle image taken at unit cell six shows the emergence of these streaks. As deposition continues, these streaks increase in intensity, as shown in the bottom image taken after 60 unit cells. Additionally, the reciprocal space map shows the film (206) diffraction spot (left) near the $SrTiO_3$(103) diffraction spot (right), with a clear gap in Q_x corresponding to in-plane relaxation of the film. This behavior agrees with previous results that demonstrate a reconstruction that occurs at the interface between $SrTiO_3$ and $BaBiO_3$ to relieve the high strain.[17]

Furthermore, we synthesize $BaBiO_3$ on (100)-oriented BaF_2 substrates. Figure 2a includes an X-ray diffraction scan of $BaBiO_3/BaF_2$. Figure 2c demonstrates the advantage of BaF_2 over $SrTiO_3$: the reciprocal space map for $BaBiO_3/BaF_2$ (blue) shows an in-plane lattice match; and electron diffraction images of $BaBiO_3$ grown on BaF_2 show a consistent lattice spacing between the substrate, the film at six unit cells, and the film at 30 unit cells. A prior finding used buffer layers to enable epitaxially strained films of $BaBiO_3$.[21] To the best of our knowledge this is the first synthesis of $BaBiO_3$ on BaF_2. Out of plane lattice parameters extracted from the XRD data in Figure 2 are shown in Table 1.[22]

We now turn to the ex situ fluorination of our oxide films. Chikamatsu et al. reported in a previous work on the fabrication of $BaBiF_5$ samples from $BaBiO_3$ precursors using

https://doi.org/10.1021/acsomega.4c05872
ACS Omega 2024, 9, 39082−39087

Table 1. Nelson-Riley *c* Lattice Parameters Extracted from XRD Measurements Shown in Figure 2

sample	*c*, measured (Å)
$BaBiO_3/SrTiO_3$	4.334 ± 0.002
$BaBiO_3/BaF_2$	4.358 ± 0.015
$SrBiO_3/SrTiO_3$	4.242 ± 0.007

poly(vinylidene fluoride) (PVDF).[10] We found that for $BaBiO_3$, using ZnF_2 as our fluoride agent allowed lower temperature fluorination and resulted in fluorinated films of higher quality compared to those using PVDF. For $SrBiO_3$, only fluorinations using PVDF resulted in $SrBiF_5$ samples demonstrating crystalline diffraction; attempts with ZnF_2 consistently led to the loss of X-ray diffraction peaks or incomplete fluorination.

Our fluorination results are summarized in Figure 3. We formed $BaBiF_5$ structures on both $SrTiO_3$ and BaF_2 substrates,

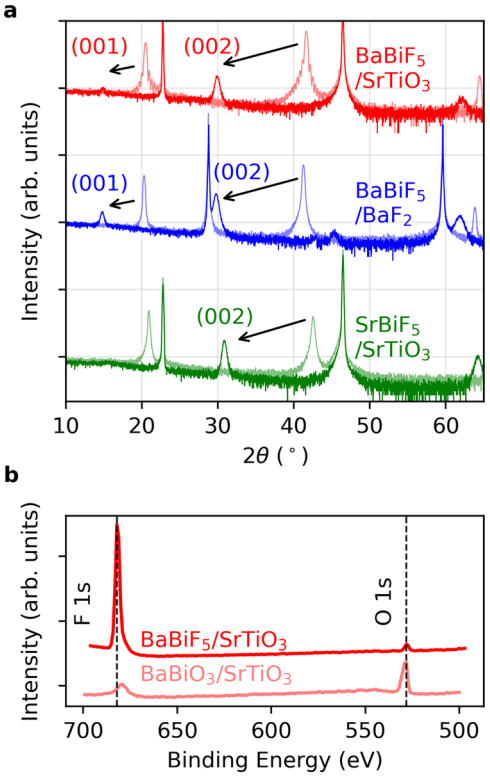

Figure 3. Fluorination of $BaBiO_3$ and $SrBiO_3$. (a) X-ray diffraction measurements of $BaBiF_5$ (top and middle) and $SrBiF_5$ (bottom). Scans of the precursor oxide phases are shown in lighter color, with arrows depicting movement of the film diffraction peaks. (b) X-ray photoelectron spectroscopy measurements of $BaBiO_3$ and $BaBiF_5$ samples. Note the decrease in intensity of the oxygen peak and the appearance of the fluorine peak after fluorination.

as well as $SrBiF_5$ on $SrTiO_3$. While $BaBiF_5$ samples demonstrate (001) diffraction peaks indicative of preserved cation ordering, $SrBiF_5$ samples did not possess such a peak. This is likely because fluorination of $SrBiO_3$ required slightly higher temperatures than that of $BaBiO_3$, potentially resulting in cation disorder.[10] A previous study on solid solutions of $Ba_{1-x}Bi_xF_{2+x}$ demonstrated two additional interstitial sites occupied by fluoride ions in addition to the normal CaF_2-structure sites.[9] Although the study only characterized solid solutions with $x < 0.45$, the prior observed distribution of fluoride ion occupation may occur in our samples as well.

To analyze how complete the fluorination process was, we performed X-ray photoelectron spectroscopy (XPS) measurements of films before and after fluorination. The barium 3d peaks were used to align the binding energy values and scale the measurement intensities for comparison. These results are shown in Figure 3b. $BaBiO_3$ demonstrates a clear oxygen 1s peak at 528 eV, as well as a bismuth $4p_{3/2}$ peak at 678 eV. This bismuth peak overlaps with the fluorine 1s peak, but as we see in the $BaBiF_5$ scan, the fluorine 1s peak has a much higher intensity. Although the peak of oxygen 1s peak is largely reduced after fluorination, there is still intensity in the fluorinated phase, indicating the presence of some oxygen. A similar result was found by Chikamatsu et al., with traces of oxygen present after fluorination.[10] Peak fitting suggests a fluorine/oxygen ratio of 14:1 in the $BaBiF_5$ sample, suggesting primarily a $BaBiF_5$ structure with oxygen impurities on about 7% of anion sites.

Now that we have successfully synthesized the fluoride compounds $BaBiF_5$ and $SrBiF_5$, we turn to characterizing the ionic conductivity of our samples with electrochemical impedance spectroscopy measurements. Figure 4a demonstrates Nyquist plots (top panel) of EIS scans taken from room temperature (about 20 °C) up to 90 °C. We observe a room temperature conductivity of 2.4×10^{-5} S/m for $BaBiF_5$. Although resistance increases somewhat for intermediate temperatures, the resistance quickly falls around 50 °C. By about 80 °C, the resistance reaches a minimum. The maximum conductivity we observe for $BaBiF_5$ is 3.4×10^{-5} S/m at 80 °C. As described above, the resistance measurements were taken in a two terminal setup. The measured resistance values therefore include contributions from contact resistances. As a result, our reported conductivity values are lower bound estimates.

To extract activation energy values, we created Arrhenius plots from the EIS data. These results are shown in Figure 4c. Ionic conductivity of electrolytes tends to follow an exponential function of the form $\sigma \propto T^n e^{-\Delta/k_B T}$, where Δ represents an activation energy and n is frequently taken to be -1.[6,23] By plotting $\log \sigma T$ versus $1/T$, we should expect linear behavior if we assume the above equation holds, with the slope of the best fit line given by Δ/k_B. Looking at our Arrhenius plot in Figure 4c, we see approximately linear behavior from 40 to 70 °C, suggesting that our Arrhenius model is appropriate in this temperature regime. A linear fit in this region suggests an activation energy of $\Delta = 240$ meV, a value comparable to or lower than other solid fluoride-ion electrolytes.[6,23] The low activation energy and related high room-temperature ionic conductivity of $BaBiF_5$ compared to existing solid fluoride-ion electrolytes supports the applicability of this barium bismuth fluoride compound as a fluoride-ion electrolyte. We observe nonlinear behavior at temperatures below 40 °C (where the resistance increases with increasing temperature) and above 70 °C (where the resistance plateaus). There are several possible interpretations of this finding. Contact resistance from our two terminal setup may be contributing metallic scattering, which would lead to a resistance component that increases with temperature. Additionally, the electrolyte may be air sensitive at elevated temperatures—the film may be slowly losing fluorine or reoxidizing. Further work is needed to deduce the true origin of this trend.

We show the same measurements and analysis on a $SrBiF_5$ sample in Figure 4b. $SrBiF_5$ demonstrates higher resistances

https://doi.org/10.1021/acsomega.4c05872
ACS Omega 2024, 9, 39082−39087

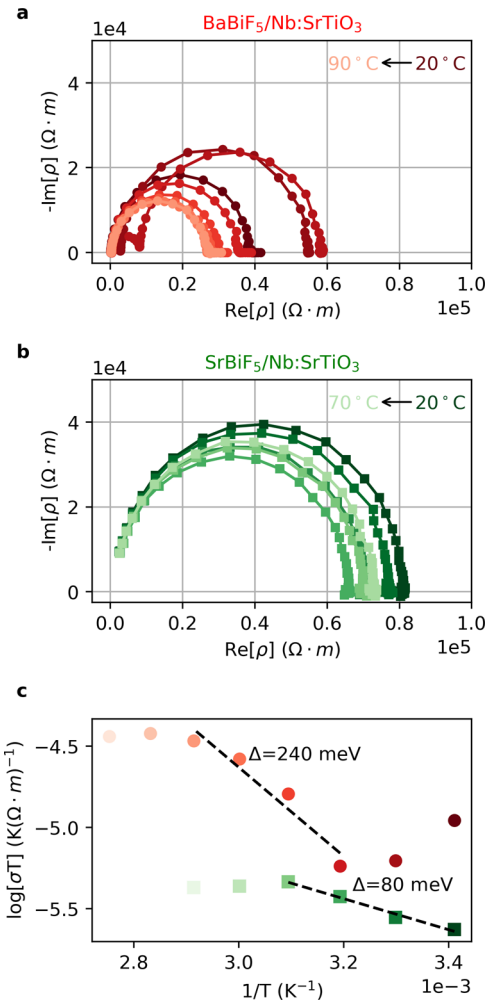

Figure 4. Electrochemical impedance spectroscopy measurements of alkaline earth bismuth fluoride films. (a) Nyquist plot of a $BaBiF_5$/Nb:$SrTiO_3$ sample. Frequency scans were taken at a range of temperatures from room temperature (20 °C) to 90 °C. (b) Nyquist plot of a $SrBiF_5$/Nb:$SrTiO_3$ sample, for temperatures up to 70 °C. Notice the higher resistivity values for $SrBiF_5$ compared with $BaBiF_5$ above. (c) Arrhenius plots of the data sets shown in **a** and **b**. Dashed lines represent linear fits over temperature regimes with roughly linear behavior.

across the board compared to $BaBiF_5$, as seen by comparing the Nyquist plots. This may be due to the smaller lattice parameter of $SrBiF_5$ given the interplay between lattice size and ionic conductivity.[24] $SrBiF_5$ demonstrates a room temperature conductivity of 1.2×10^{-5} S/m, about half of the value measured for $BaBiF_5$. The Arrhenius plot in Figure 4c shows weaker ionic conductivity in $SrBiF_5$. A linear fit results in an activation energy of $\Delta = 80$ meV, lower than in $BaBiF_5$, despite the fact that $SrBiF_5$ also demonstrates lower conductivities. Similar to $BaBiF_5$, $SrBiF_5$ demonstrates a plateau in the Arrhenius plot for temperatures above 50 °C.

In conclusion, we demonstrate the synthesis of the thin film fluoride compounds $BaBiF_5$ and $SrBiF_5$, including the realization of $BaBiF_5$ on BaF_2 substrates. EIS measurements show thermal activation in both materials, with higher conductivities present in $BaBiF_5$. Although our measured conductivity values are about 3 orders of magnitude lower than other fluoride-ion electrolytes, we suspect that the conductivity can be increased, for example along in plane directions where fluoride-ions likely have more connected conduction pathways as seen in Figure 1. Additionally, nonlinearities in our Arrhenius plots suggest external contributions to our measured resistances, such as high contact resistance. Further work could compare ionic conductivity along different crystallographic directions, and as a function of disorder. With the demonstration of these materials as functioning fluoride-ion electrolytes, we propose straightforward battery stacks Bi/$BaBiF_5$/BaF_2 and Bi/$SrBiF_5$/SrF_2, systems which may advance the field's progress toward scalable room-temperature fluoride-ion batteries.

■ ASSOCIATED CONTENT

Data Availability Statement

Data is available throughout the manuscript and supporting files. Files containing data presented in the figures and other findings of this study are available from the corresponding authors upon reasonable request.

Supporting Information

The Supporting Information is available free of charge at https://pubs.acs.org/doi/10.1021/acsomega.4c05872.

Details on the synthesis of $BaBiO_3$ and $SrBiO_3$ thin films (PDF)

■ AUTHOR INFORMATION

Corresponding Author

Julia A. Mundy − *Department of Physics, Harvard University, Cambridge, Massachusetts 02138, United States;* orcid.org/0000-0001-8454-0124; Email: mundy@fas.harvard.edu

Authors

Spencer Doyle − *Department of Physics, Harvard University, Cambridge, Massachusetts 02138, United States;* orcid.org/0000-0002-6596-8683

Edvin Tewolde Berhane − *Department of Physics, Harvard University, Cambridge, Massachusetts 02138, United States*

Peichao Zou − *Department of Physics and Astronomy, University of California, Irvine, California 92697, United States*

Ari B. Turkiewicz − *Department of Physics, Harvard University, Cambridge, Massachusetts 02138, United States;* orcid.org/0000-0001-5729-0289

Yang Zhang − *The Rowland Institute at Harvard, Harvard University, Cambridge, Massachusetts 02142, United States*

Charles M. Brooks − *Department of Physics, Harvard University, Cambridge, Massachusetts 02138, United States*

Ismail El Baggari − *The Rowland Institute at Harvard, Harvard University, Cambridge, Massachusetts 02142, United States*

Huolin L. Xin − *Department of Physics and Astronomy, University of California, Irvine, California 92697, United States*

Complete contact information is available at: https://pubs.acs.org/10.1021/acsomega.4c05872

Author Contributions

S.D., E.T.B., C.M.B. and J.A.M. synthesized the thin-films. P.Z., H.L.X., and S.D. performed the electrical impedance measurements. S.D., E.T.B., and C.M.B. performed X-ray diffraction measurements. A.B.T., S.D., and E.T.B. performed topotactic fluorinations. E.T.B. performed X-ray photoelectron spectros-

https://doi.org/10.1021/acsomega.4c05872
ACS Omega 2024, 9, 39082−39087

copy measurements. Y.Z. and I.E.B. characterized the samples with scanning transmission electron microscopy. S.D., A.B.T., and J.A.M. conceived and guided the study. S.D. and J.A.M. wrote the manuscript with discussion and contributions from all authors.

Notes

The authors declare no competing financial interest.

■ ACKNOWLEDGMENTS

Research is primarily supported by the National Science Foundation with award DMR-2323970. We acknowledge funding from the Star Friedman Fund at Harvard University. Device fabrication work was performed at Harvard University's Center for Nanoscale Systems (CNS), a member of the National Nanotechnology Coordinated Infrastructure Network (NNCI), supported by the National Science Foundation under NSF Grant No. 1541959. S.D. acknowledges support from the NSF Graduate Research Fellowship Grant No. DGE-1745303. H.L.X. acknowledges the unrestricted funding provided by UC Irvine. J.A.M acknowledges support from the Packard Foundation and Gordon and Betty Moore Foundations EPiQS Initiative, Grant GBMF6760.

■ REFERENCES

(1) Blair, N.; Augustine, C.; Cole, W.; Denholm, P.; Frazier, W.; Geocaris, M.; Jorgenson, J.; McCabe, K.; Podkaminer, K.; Prasanna, A.; Sigrin, B. *Storage Futures Study: Key Learnings for the Coming Decades*; National Renewable Energy Lab.(NREL): Golden, CO, United States, 2022.

(2) Greim, P.; Solomon, A. A.; Breyer, C. Assessment of lithium criticality in the global energy transition and addressing policy gaps in transportation. *Nat. Commun.* **2020**, *11*, No. 4570, DOI: 10.1038/s41467-020-18402-y.

(3) Kalantzakos, S. The Race for Critical Minerals in an Era of Geopolitical Realignments. *Int. Spectator* **2020**, *55*, 1−16.

(4) Xiao, A. W.; Galatolo, G.; Pasta, M. The case for fluoride-ion batteries. *Joule* **2021**, *5*, 2823−2844.

(5) Reddy, M. A.; Fichtner, M. Batteries based on fluoride shuttle. *J. Mater. Chem.* **2011**, *21*, 17059−17062.

(6) Mohammad, I.; Witter, R.; Fichtner, M.; Reddy, M. A. Room-Temperature, Rechargeable Solid-State Fluoride-Ion Batteries. *ACS Appl. Energy Mater.* **2018**, *1*, 4766−4775.

(7) Zhang, M.; Cao, X.; Hao, Y.; Wang, H.; Pu, J.; Chi, B.; Shen, Z. Recent progress, challenges and prospects of electrolytes for fluoride-ion batteries. *Energy Rev.* **2024**, *3*, No. 100083.

(8) Reau, J.; Tian, S. B.; Rhandour, A.; Matar, S.; Hagenmuller, P. Respective influence of optimization criteria on transport properties of $Ba_{1-x}M'_xF_{2+x}$ solid solution (M′=In, Bi). *Solid State Ionics* **1985**, *15*, 217−223.

(9) Soubeyroux, J.; Réau, J.; Wahbi, M.; Sénégas, J.; Soo, S. K. Neutron diffraction investigation of the $Ba_{1-x}Bi_xF_{2+x}$ solid solution. *Solid State Commun.* **1992**, *82*, 63−70.

(10) Chikamatsu, A.; Kawahara, K.; Shiina, T.; Onozuka, T.; Katayama, T.; Hasegawa, T. Fabrication of Fluorite-Type Fluoride $Ba_{0.5}Bi_{0.5}F_{2.5}$ Thin Films by Fluorination of Perovskite $BaBiO_3$ Precursors with Poly(vinylidene fluoride). *ACS Omega* **2018**, *3*, 13141−13145.

(11) Slater, P. Poly(vinylidene fluoride) as a reagent for the synthesis of K2NiF4-related inorganic oxide fluorides. *J. Fluorine Chem.* **2002**, *117*, 43−45.

(12) Katayama, T.; Chikamatsu, A.; Hirose, Y.; Takagi, R.; Kamisaka, H.; Fukumura, T.; Hasegawa, T. Topotactic fluorination of strontium iron oxide thin films using polyvinylidene fluoride. *J. Mater. Chem. C* **2014**, *2*, 5350−5356.

(13) Moon, E. J.; Xie, Y.; Laird, E. D.; Keavney, D. J.; Li, C. Y.; May, S. J. Fluorination of Epitaxial Oxides: Synthesis of Perovskite Oxyfluoride Thin Films. *J. Am. Chem. Soc.* **2014**, *136*, 2224−2227.

(14) Sun, J.; Parzyck, C. T.; Lee, J. H.; et al. Canonical approach to cation flux calibration in oxide molecular-beam epitaxy. *Phys. Rev. Mater.* **2022**, *6*, No. 033802.

(15) Lasia, A. *Electrochemical Impedance Spectroscopy and its Applications*; Springer: New York, 2014.

(16) Lazanas, A. C.; Prodromidis, M. I. Electrochemical Impedance Spectroscopy-A Tutorial. *ACS Meas. Sci. Au* **2023**, *3*, 162−193.

(17) Zapf, M.; Stübinger, M.; Jin, L.; Kamp, M.; Pfaff, F.; Lubk, A.; Büchner, B.; Sing, M.; Claessen, R. Domain matching epitaxy of $BaBiO_3$ on $SrTiO_3$ with structurally modified interface. *Appl. Phys. Lett.* **2018**, *112*, No. 141601.

(18) Nowroozi, M. A.; Mohammad, I.; Molaiyan, P.; Wissel, K.; Munnangi, A. R.; Clemens, O. Fluoride ion batteries past, present, and future. *J. Mater. Chem. A* **2021**, *9*, 5980−6012.

(19) Zapf, M.; Elsässer, S.; Stübinger, M.; Scheiderer, P.; Geurts, J.; Sing, M.; Claessen, R. Structural and stoichiometric modifications in ultrathin epitaxial $BaBiO_3$ films. *Phys. Rev. B* **2019**, *99*, No. 245308.

(20) Li, F.; Davidson, B. A.; Sutarto, R.; Shin, H.; Liu, C.; Elfimov, I.; Foyevtsova, K.; He, F.; Sawatzky, G. A.; Zou, K. Epitaxial growth of perovskite $SrBiO_3$ film on $SrTiO_3$ by oxide molecular beam epitaxy. *Phys. Rev. Mater.* **2019**, *3*, No. 100802.

(21) Lee, H. G.; Kim, Y.; Hwang, S.; Kim, G.; Kang, T. D.; Kim, M.; Kim, M.; Noh, T. W. Double-layer buffer template to grow commensurate epitaxial BaBiO3 thin films. *APL Mater.* **2016**, *4*, No. 126106.

(22) Nelson, J. B.; Riley, D. P. An experimental investigation of extrapolation methods in the derivation of accurate unit-cell dimensions of crystals. *Proc. Phys. Soc.* **1945**, *57*, No. 160.

(23) Tachibana, S.; Zhong, C.; Ide, K.; Yamasaki, H.; Tojigamori, T.; Miki, H.; Saito, T.; Kamiyama, T.; Shimoda, K.; Orikasa, Y. Fluorosulfide $La_{2+x}Sr_{1-x}F_{4+x}S_2$ with a Triple-Fluorite Layer Enabling Interstitial Fluoride-Ion Conduction. *Chem. Mater.* **2023**, *35*, 4235−4242.

(24) Bachman, J. C.; Muy, S.; Grimaud, A.; Chang, H.-H.; Pour, N.; Lux, S. F.; Paschos, O.; Maglia, F.; Lupart, S.; Lamp, P.; Giordano, L.; Shao-Horn, Y. Inorganic Solid-State Electrolytes for Lithium Batteries: Mechanisms and Properties Governing Ion Conduction. *Chem. Rev.* **2016**, *116*, 140−162.

https://doi.org/10.1021/acsomega.4c05872
ACS Omega 2024, 9, 39082−39087